Properties of MoO_3 Nanostructures Grown Via Thermal Oxidation

Viorel TROFIM[1], Vasilii CREŢU[1], Oleg LUPAN[1], Ivan STAMOV[2], Nicolae SYRBU[1], Victor ZALAMAI[3], Lee CHOW[4]

[1]*Technical University of Moldova*
[2]*Tiraspol State University of Moldova*
[3]*Academy of Sciences of Moldova*
[4]*University of Central Florida, USA*
vgtrofim@yahoo.com

***Abstract* — Metal oxides such as molybdenum oxide (MoO_3) have been studied intensively as sensors and electrochromic systems during of the last decade. MoO_3 nanowires present new properties at nanometer dimensions. Its structural, morphological and optical properties were studied by using X-ray diffraction (XRD), scanning electron microscopy (SEM), micro-Raman and optical transmission techniques. This work demonstrates properties MoO_3 nanostructures grown via thermal oxidation which is rapid and cost-effective technological procedure. It is shown that MoO_3 consisted of stratified long rectangles and nanowires, may be used in sensor structures and other applications.**

***Index Terms* — MoO_3, nanowires, sensor, molybdenum trioxide.**

I. INTRODUCTION

Metal oxide thin films have been extensively studied and used in gas sensors due to conductance changes when it interacts with gas molecules [1]. Such sensor structures offers easy fabrication, low-cost and consistent performances with respect to different types of gasses investigated. Recently, an increased trend to use specifically engineered nanostructured materials for gas sensor applications is noted [2]. Hydrogen (H_2) sensors are extensively used in certain types of combustion systems of cars to monitor pollution, as well as in the chemical, or semiconductor industries [3-4]. Nanostructures, such as nanobelts, nanorods, and nanowires offer higher surface-to-volume ratio and unique structural properties that are expected to enhance the gas sensor performances.

In this context, molybdenum trioxide MoO_3 – a metal oxide material with semiconductor properties and a wide band gap of about 2.4-2.9 eV is an excellent candidate for electrochromic and gas sensing applications [5]. Research works were performed to study the gas sensing characteristics of MoO_3-based sensors to detect H_2 [6], NH_3 [7], liquid petroleum gas LPG [6], etc.

Multiple techniques were reported for the deposition of MoO_3, such as thermal evaporation [8], sputtering [9], spray pyrolysis [10], electrodeposition [11], hydrothermal [12], solution method [13], etc. We found that the synthesis of MoO_3 via evaporative techniques or thermal oxidation are attractive for mass-production of highly crystalline and stratified structures. This is very important since higher crystallinity and layered formations allow a greater gas response. Although, previous publications on pure MoO_3 nanostructure-based H_2 sensors showed the promise of such devices in commercial sensing applications, their relative slow response and recovery times are major drawbacks for their implementation in an industrial setting. A rapid thermal oxidation technique is required to control morphologies of MoO_3 and to growth higher crystal quality nanomaterial. In addition more research work is required to enhance gas sensitivity, selectivity, stability and faster gas responses by precise control of material morphology and properties. Improvements in the performance of MoO_3 sensors can be achieved high surface-to-volume ratio and high quality material obtained by a cost effective technique.

In this work we used a rapid thermal oxidation (RTO) method for the synthesis of MoO_3 nanowires and microbelts. Samples of MoO_3 nano-micro-structures were characterized using scanning electron microscopy (SEM), energy dispersive X-ray spectroscopy (EDX), X-ray powder diffraction (XRD), micro-Raman spectroscopy, and optical transmission techniques.

II. EXPERIMENTAL

The growth of MoO_3 nanostructures were made by thermal oxidation RTO at 1000 °C for 0.2 h.

The as-grown samples were characterized by scanning electron microscopy. SEM images were acquired with an Ultra 55 Zeiss FEG at an acceleration voltage of 15 kV. The compositional analysis of ZnO nanorods was carried out using Energy dispersive X-ray spectroscopy, in combination with SEM. X-ray powder diffraction (Rigaku 'DB/MAX' powder diffractometer) was used for structural analysis and identification of phases for Bragg angles (2θ) ranging from 10° to 95° using Cu Kα radiation (λ = 1.54178 Å). Details of the experimental procedures can be found in our report [4]. Information on vibrational modes in pure MoO_3 nanostructures was obtained from Raman backscattering experiments in a micro-Raman setup Horiba Jobin Yvon LabRam IR spectrometer with a charge-coupled detector (CCD). Raman spectra were excited with 1.96 eV photons from a Helium Neon laser (λ~632.8 nm) with less than 4 mW of power at the sample. The spectral resolution was 2 cm^{-1},

and the instrument was calibrated using silicon and a naphthalene standards.

The optical properties of these materials were studied by using set-up described in [2] and references therein. The samples were mounted on the cold station of a LTS-22-C-330 optical cryogenic system for optical studies at 10K.

III. RESULTS AND DISCUSSIONS

Figure 1 show the X-ray diffraction XRD pattern recorded in the range of 10-95° with a scanning step of 0.02° of MoO_3 depositions. XRD studies of the crystal structure indicate only MoO_3 peaks, which are intense and well-defined diffraction lines. For evaluation of lattice parameters the following relation is used:

$$d_{\mathrm{hkl}} = \frac{1}{\sqrt{\frac{h^2}{a^2} + \frac{k^2}{b^2} + \frac{l^2}{c^2}}} \quad (1)$$

with *a*#*b*#*c* for orthorhombic lattice. Parameter d_{hkl} is interreticular distance, (*h*, *k*, *l*) are Miller indices of reflector planes appearing on the diffraction spectrum. The obtained lattice parameters are *a* = 0.3962 nm, *b* = 1.3858 nm, *c* = 0.3697 nm, which are in good agreement with reported data [14]. The pattern matches the lattice spacing of crystalline molybdenum oxide in the orthorhombic structure (α-MoO_3, lattice parameters of *a* = 0.3962 nm, *b* = 1.3858 nm, *c* = 0.3697 nm). The data are in agreement with the Joint Committee on Diffraction Standards (JCPDS, Card #005-0508). It can be seen that XRD pattern from this sample shows predominant (040) diffraction peaks [15] as preferred orientation. The strong diffractions peaks of MoO_3 corresponds to (020), (040), (060) and (081) planes. Weaker XRD peaks are assigned to MoO_3 (110), (021), (190) and (0100) planes. These XRD peaks were compared to literature and indicate the existence of orthorhombic MoO_3 structure and α-phase. The strong intensity of the XRD reflection peaks of (0*k*0) with *k*=2, 4, 6 proves the existence of the lamellar structure [16]. These results demonstrate a high degree of crystallinity.

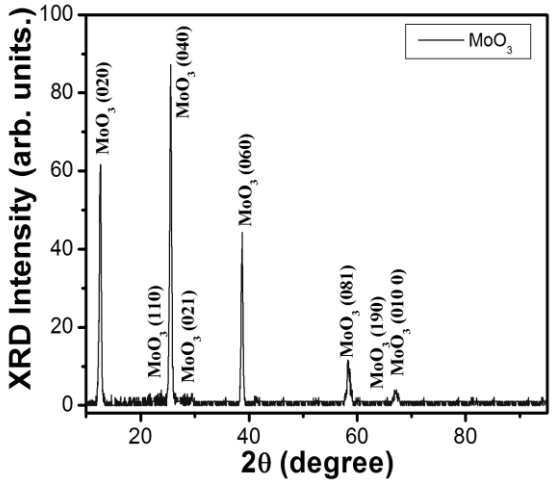

Fig. 1. X-ray diffraction XRD pattern of MoO_3 structures.

Figure 2(a) presents a low-magnification SEM image of the samples prepared at 1000 °C on a Si substrate. It can be seen that these products have uniform lengths of about few hundred μm and diameters of 50–2000 nm. MoO_3 nanowire on Si substrate is shown in Figure 1(b). Microbelts, large rectangular plates and nanowires are the main shapes of the as grown MoO_3 structures via rapid thermal oxidation RTO in 0.2 h.

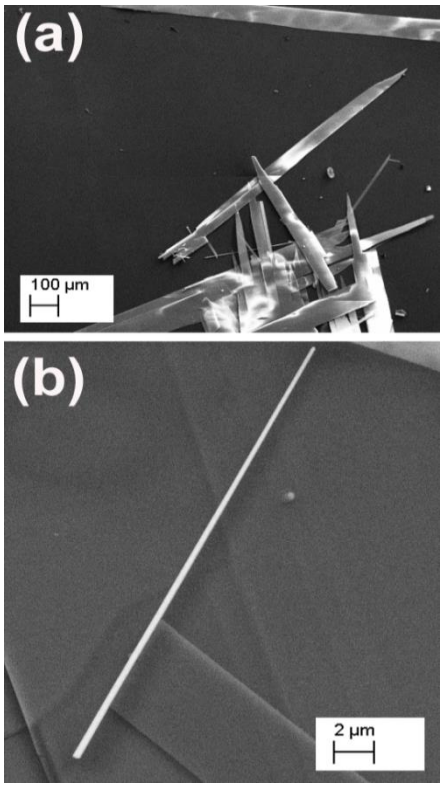

Fig. 2. (a) SEM image of MoO_3 structures transferred to Si substrate. (b) Transferred MoO_3 nanowires from initial products. These nanowires and microbelts can be used as building nanoblocks for sensors structures.

EDX indicates a stoichiometric MoO_3 and its electrical characteristics (not shown) demonstrate a large electrical resistance, which confirms that it is an insulator.

The Micro-Raman spectrum of the MoO_3 nanostructures at room temperature is shown in Figure 3. It can be concluded that all peaks are in good agreement with the previously reported orthorhombic MoO_3 crystal material and assigned to vibrational modes of MoO_3 [7,17-18].

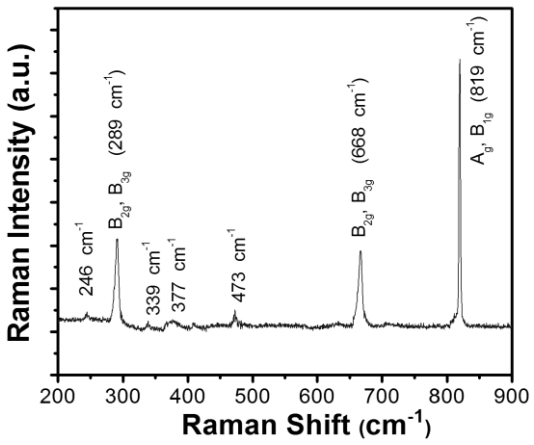

Fig. 3. Raman spectrum of MoO_3 nanostructures measured in air at room-temperature.

Peak at the 995 cm^{-1} (A_g, B_{1g}) (not shown) is the asymmetric stretch of the terminal oxygen atoms [17-18]. Peaks at the 819 cm^{-1} (A_g, B_{1g}) is a symmetric stretch of the terminal oxygen atoms, at the 668 cm^{-1} (B_{2g}, B_{3g}) to an asymmetric stretching Mo–O–Mo bridge along the *c*-axis, and at the 473 cm^{-1} to Mo-O stretching and bending mode of MoO_6 octahedra. Peaks at the 378 cm^{-1} and 338 cm^{-1} correspond to various bending modes of the orthorhombic MoO_3 crystal. The 289 cm^{-1} (B_{2g}, B_{3g}) band is a doublet comprised of wagging modes of the terminal oxygen atoms [17-18].

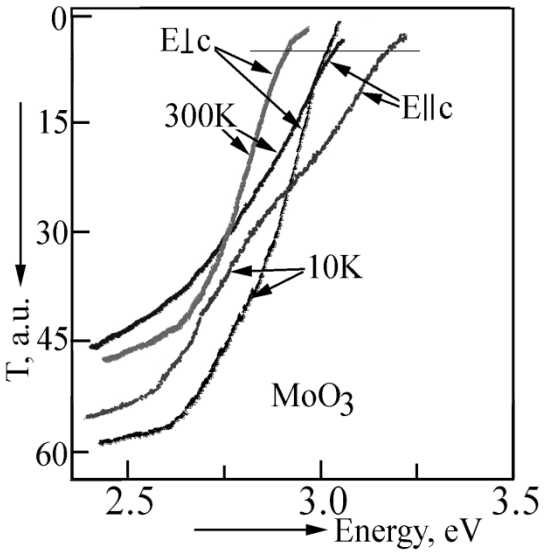

Fig. 4. Transmission spectra of MoO_3 crystals as a function of photon energy.

Transmission spectra of the crystals MoO_3 thick 547mk in near-band edge absorption 2.5 - 3.2 eV are shown in Figure 4. Transmission spectra for polarizations E||c and E⊥c at 300 K and 10 K intersect. The spectra indicate that the minimum interband period is formed by polarized transitions. According to theoretical calculations, the minimum interband gap formed indirect transitions [19]. From the results shown in Figure 4, it is concluded that the band gap in the polarization E⊥c is smaller than in case with polarization E||c. As the temperature decreases the absorption edge shifts to higher energy saving polarization dependence. Absorption edge shift $\beta=\Delta E/\Delta T$ for the polarization E⊥c (at 5 rel.un.T) is $3{,}6\times10^{-4}$ eV/K and in the case of E||c is $4{,}7\times10^{-4}$ eV/K. The splitting of the absorption edge at the level of 5 rel.un.T at 300 K and 10 K are 0.123 eV and 0.156 eV, respectively. Consequently, the minimum inter-band gap in the polarization E⊥c formed from indirect transitions from the zone V_1 of point R of the Brillouin zone in the zone C1 of point Γ of the Brillouin zone. In the polarization E‖c, the band gap width is also formed by indirect transitions from point R to point Γ from zones V2 to C2.

Figure 5 shows the first derivative of the energy of the transmission spectra of crystals MoO_3 547mk thickness at 300 K for the polarizations E⊥c and E||c. The derivative of the transmission energy intersects with the axis $(\Delta T/\Delta E)=0$ at the energy 2.914 eV (E⊥c), with energy 3.037 eV (E||c). These values correspond to the indirect band gap in the respective polarizations. Particularly weak α1, α2, α3 and β1 may due to absorption and emission of phonons in indirect transitions. Assuming that α1 (2,939 eV) and α2 (3,032 eV) is due to indirect transitions with the absorption and emission of phonons, the phonon energy is approximately equal to 46.5 meV (376 cm^{-1}). In crystals phonon MoO_3 in the high-frequency region can be observed phonons with 365 cm^{-1}, and 376 cm^{-1}.

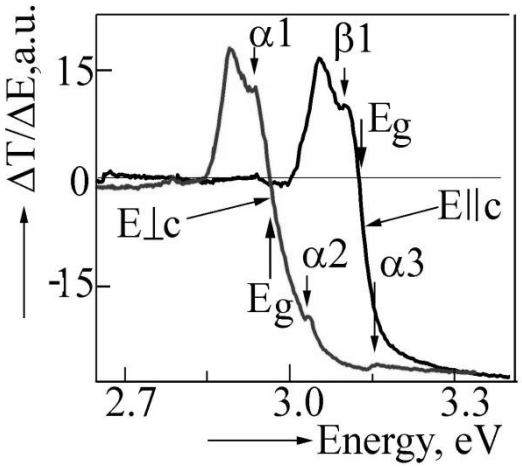

Fig. 5. The derivative of the energy of the transmission spectra of crystals MoO_3 thick 547 mk as a function of energy.

From the grown nanocrystalline MoO_3, we were able to measure the transmission spectra of crystals of thickness 1.7 microns at room (300 K) and low temperatures (10 K). The transmission spectrum reveals a characteristic interference Fabry Perot (see Figure 6).

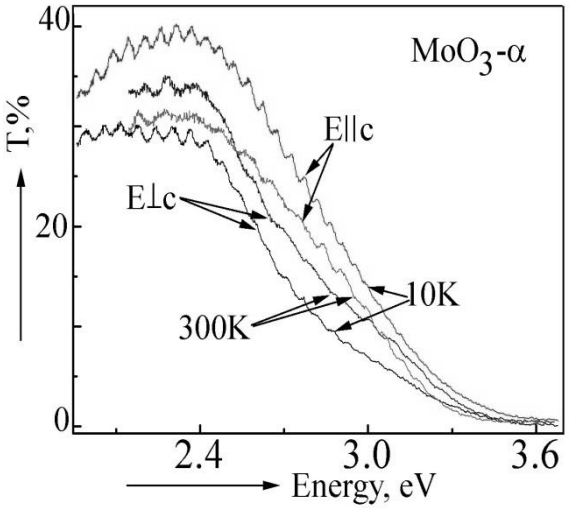

Fig. 6. Transmission spectra of MoO_3 crystal thickness 1.7 microns as a function of photon energy.

From these data refractive indices were calculated for polarizations E⊥c and E||c which vary from 2 to 2.8, and double-cross, Figure 7. These results are in good agreement with those of reported in [20].

IV. CONCLUSION

In summary, we have investigated properties of MoO_3 micro-nano-structures and observed orthorhombic structure of α-MoO_3. The corresponding optical band gap

energies are in the typical range for crystalline MoO_3 (2.7–2.9 eV). The values of the optical band gap for different polarizations differ significantly. From the transmission spectra can be concluded that the band gap in the polarization E⊥c is smaller than in case with polarization E||c. With decreasing sample temperature was observed a shift of absorption edge to a higher energy saving polarization dependence. The transmission spectrum reveals a characteristic interference Fabry Perot.

The observation of their performances suggests the promising application of MoO_3 nanostructures in sensorial nanodevices and other applications.

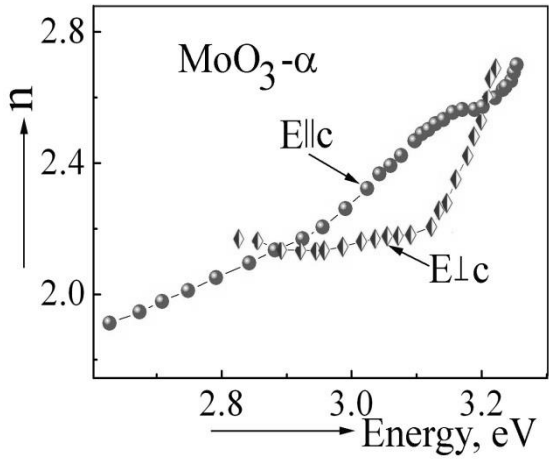

Fig. 7. The refractive index of MoO_3 crystal thickness 1.7 microns.

ACKNOWLEDGMENTS

This research was performed with the financial support of the STCU and ASM through Grant 09 STCU.A/5833.

REFERENCES

[1] G. Korotcenkov, "Metal oxides for solid-state gas sensors: What determines our choice?" *Materials Science and Engineering B*, vol. 139, pp. 1–23, 2007.

[2] I. M. Tiginyanu, O. Lupan, V. V. Ursaki, L. Chow, M. Enachi, "Nanostructures of Metal Oxides." *Comprehensive Semiconductor Science & Technology*, Chapter 3.11, pp. 396-479, 2011.

[3] T. Hübert, L. Boon-Brett, G. Black and U. Banach, "Hydrogen sensors – A review," *Sensors and Actuators B,* vol. 157, pp. 329– 352, 2011.

[4] O. Lupan, L. Chow, Th. Pauporté, L. K. Ono, B. Roldan Cuenya, G. Chai, "Highly sensitive and selective hydrogen single-nanowire nanosensor," *Sensors and Actuators B: Chemical*, vol. 173, pp. 772-780, 2012.

[5] M. B. RahmaniAuthor Vitae, S.H. KeshmiriAuthor Vitae, J. YuAuthor Vitae, A. Z. SadekAuthor Vitae, L. Al-MashatAuthor Vitae, A. MoafiAuthor Vitae, K. LathamAuthor Vitae, Y. X. LiAuthor Vitae, W. WlodarskiAuthor Vitae, K. Kalantar-zadeh, "Gas sensing properties of thermally evaporated lamellar MoO3**,"** *Sensors and Actuators B,* vol 145, pp. 13-19, 2010.

[6] S. S Sunu, E. Prabhu, V. Jayaraman, K. Gnanasekar, T. Seshagiri, T. Gnanasekaran, "Electrical conductivity and gas sensing properties of MoO3," *Sensors and Actuators B: Chemical*, vol. 101, pp. 161-174, 2004.

[7] C. Imawan, F. Solzbacher, H. Steffes, E. Obermeier, "Gas-sensing characteristics of modified-MoO3 thin films using Ti-overlayers for NH3 gas sensors," *Sensors and Actuators B*, vol. 64, pp. 193–197, 2000.

[8] J. Zhou, S. Z. Deng, N. S. Xu, J. Chen, J. C. She, "Synthesis and fieldemission properties of aligned MoO3 nanowires," *Appl. Phys. Lett.*, vol. 83, pp. 2653–2655, 2003.

[9] C. Imawan, H. Steffes, F. Solzbacher, E. Obermeier, "A new preparation method for sputtered MoO3 multilayers for the application in gas sensors," *Sensors and Actuators B*, vol. 78, pp. 119–125, 2001.

[10] A. Bouzidi, N. Benramdane, H. Tabet-Derranz, C. Mathieu, B. Khelifa, R. Desfeux, "Effect of substrate temperature on the structural and optical properties of MoO3 thin films prepared by spray pyrolysis technique," *Mater. Sci. Eng. B*, vol. 97, pp. 5–8, 2003.

[11] R. S. Patil, M. D. Uplane, P. S. Patil, "Structural and optical properties of electrodeposited molybdenum oxide thin films," *Appl. Surf. Sci.*, vol. 252, pp. 8050–8056, 2006.

[12] R. Q. Song, A. W. Xu, B. Deng, Y. P. Fang. "Novel Multilamellar Mesostructured Molybdenum Oxide Nanofibers and Nanobelts: Synthesis and Characterization," *J. Phys. Chem. B* vol. 109, pp. 22758-22766, 2005.

[13] R. Naouel, F. Touati, N. Gharbi, "Control of the Morphology of Molybdenum Dioxide Nanoparticles," *E-Journal of Chemistry*, ISSN:0973-4945 vol. 9(1), pp. 233-239, 2012.

[14] L. Kihlborg, *Arkiv Kemi* 21, 357, 1963.

[15] JCPDS data card no. 005- 0508.

[16] Q.P. Ding, H.B. Huang, J.H. Duan, J.F. Gong, S.G. Yang, Y.W. Du "Molybdenum trioxide nanostructures prepared by thermal oxidization of molybdenum," *J. Cryst. Growth*, vol. 294, pp. 304-308, 2006.

[17] B. C. Windom, W. G. Sawyer, D. W. Hahn, "A Raman Spectroscopic Study of MoS2 and MoO3: Applications to Tribological Systems," *Tribol. Lett*. vol. 42, pp. 301–310, 2011.

[18] G. Mestl, P. Ruiz, B. Delmon, H. Knozinger, "Oxygen-exchange properties of MoO3: an in situ Raman spectroscopy study," *J. Phys. Chem.* vol. 98, pp. 11269–11275, 1994.

[19] D. O. Scanlon, G. W. Watson, D. J. Payne, G. R. Atkinson, R. G. Egdell, D. S. L. Law, *J. Phys. Chem. C*. vol. 114, pp. 4636-4645, 2010.

[20] A. Szekeres, T. Ivanova, K. Gesheva, "Spectroscopic ellipsometry study of CVD molybdenum oxide films: effect of temperature," *J. Solid State Electrochem*, vol. 7, pp. 17-20, 2002.